Hybrid Active–passive Damping Treatment of Sandwich Beams in Non-linear Dynamics

Ana Cristina Galucio, Jean-François Deü, Roger Ohayon

Hybrid Active–passive Damping Treatment of Sandwich Beams in Non-linear Dynamics

A. C. GALUCIO
J.-F. DEÜ
R. OHAYON
Chair of Mechanics, Structural Mechanics and Coupled Systems Laboratory, Conservatoire National des Arts et Métiers (CNAM), Case courrier 353, 292 rue Saint-Martin, 75141 Paris Cedex 03, France (galucio@cnam.fr)

Abstract: In the context of large displacement and rotations, this work presents a co-rotational finite element formulation of an adaptive sandwich beam composed of a viscoelastic core constrained by laminated elastic/piezoelectric faces. A classical sandwich theory is used for the face/core/face set, considering transverse shear deformations for the core. The four-parameter fractional Zener model is used in order to take the viscoelastic behavior of the middle layer into account, while a classical linear piezoelectric constitutive law is used for modeling the piezoelectric material. The finite element formulation allows large displacements and rotations with a local small strain measure. Moreover, local electrical degrees-of-freedom are used in order to reproduce sensor configurations. Another particularity consists of approximating the fractional derivative operator by the Grünwald-Letnikov scheme, where the history of the internal memory force is used to take into account the damping effect.

Keywords: Piezoelectric patches, viscoelasticity, fractional derivatives, sandwich beam, co-rotational formulation, non-linear dynamics

1. INTRODUCTION

The interest directed to investigate flexible mechanisms undergoing large overall motions in non-linear dynamics has been increased in several industrial areas. Special attention is given for spatial (see, for example, Jonker (1989); Simo and Vu-Quoc (1988)) and planar beams (using, for example, convected coordinates (Belytschko and Hsieh, 1973), inertial frame approach (Simo and Vu-Quoc, 1986) or corotational formulation (Hsiao and Jang, 1991)). The latter has been widely investigated. Iura and Atluri (1995) developed a finite element formulation of Timoshenko beams undergoing finite rotations with small strains using inertial and rotational frames. Large rotations were also accounted for in the work developed by Meek and Liu (1995). They introduced rotary inertia effects using finite deformations for a Timoshenko beam. Further, an Euler–Bernoulli beam undergoing finite displacements and rotations was analyzed by Chen and Huang (2001). They used a slider-crank mechanism to demonstrate that high-speed applications require a non-linear strain measure.

None of the above-mentioned studies focus on vibration control aspects, which is a research topic of great interest. Three main classes of vibration control can be mentioned: passive, active and passive/active damping treatments. In the context of passive techniques, viscoelastic constrained layer damping treatments are especially widespread. For this purpose, finite elements formulations of sandwich beams have been developed, for example, for rotating beams (Lin and Chen, 2003) or high-speed flexible linkage mechanisms (Zhang and Erdman, 2001). Concerning active control using integrated/collocated piezoelectric bodies, a total Lagrangian formulation for Euler–Bernoulli beams has been developed by Preiswerk and Venkatesh (1994). They used a control law based on the placement of closed-loop poles, showing several examples of planar flexible-linkage mechanisms. In the case of more complex structures, an optimal control strategy was considered to control vibrations in spatial frames (Shi and Atluri, 1990) or shells (Tan and Vu-Quoc, 2005). Tan and Vu-Quoc (2005) presents a reduced-order model strategy, which is similar to the one proposed in this investigation.

Finally, active control can be combined with a passive treatment wherein a very popular hybrid technique is the so-called active constrained layer damping treatment. In this kind of treatment, the piezoelectric layer works as a constraining layer in order to enhance the shear deformation of the viscoelastic damping layer (Baz, 1996; Baz and Ro, 1996). In the context of non-linear dynamics, hybrid active/passive strategies are carried out using an active constrained layer damping treatment. Baz and Ro (2001) proposed a finite element formulation validated through experimental results for rotating beams wherein a proportional derivative control law is used in conjunction with a complex shear modulus model for the viscoelastic damping. More recently, Fung and Yau (2004) enhanced this formulation by introducing centrifugal stiffening effects due to the rotation of the beam as well as potential energies of the viscoelastic layer due to extension and bending. Also, the viscoelastic damping is described by a complex modulus technique. Obviously, more sophisticated viscoelastic models can be used as for example, the Golla–Hughes–McTavish (GHM) model (Sun and Tong, 2004).

In this work, a co-rotational finite element formulation of an adaptive sandwich beam composed of a viscoelastic core constrained by laminated elastic/piezoelectric faces is presented. The main motivation for developing this co-rotational formulation is to propose a general framework in which vibrations and non-linear kinematic effects are investigated together. For example, the envisioned applications are related to the vibration control of structures after an impact excitation or coupled with a fluid environment. This kind of approach can easily be enriched to take large structural deflections or centrifugal stiffening into account, although in the present work these aspects are neglected. In this investigation, a classical sandwich theory is used for the face/core/face set, considering transverse shear deformations for the core. A fractional derivative model, i.e. the four-parameter fractional Zener model (Bagley and Torvik, 1983) is used in order to take the linear viscoelastic behavior of the middle layer into account, while a classical linear piezoelectric constitutive law is used for modeling the piezoelectric material. The authors believe that there are no reports in the literature using this rheological model to describe viscoelastic damping in non-linear dynamics. The finite element formulation allows large displacements and rotations with a local small strain measure. It should be emphasized that centrifugal stiffening effects are not taken into account in this investigation since only low speed rotations are considered. Obviously, this topic might be analyzed in future works. Concerning the implementation of the constitutive laws into the co-rotational formulation, two particular features are high-

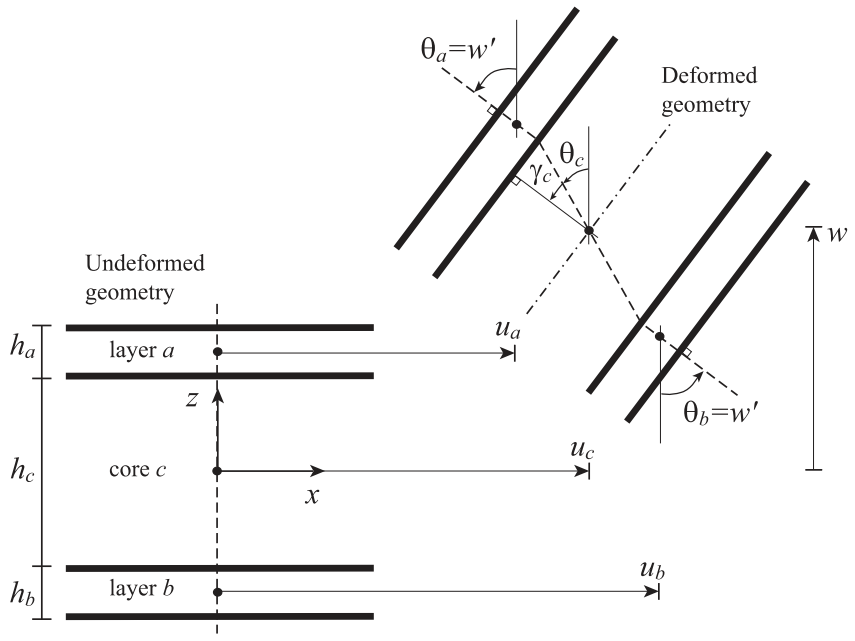

Figure 1. Kinematics of the sandwich beam.

lighted. The first one is associated with the electromechanical coupling arising from the piezoelectric material. Local electrical degrees-of-freedom are used in order to reproduce sensor configurations. The second feature is an approximation of the fractional derivative operator using the Grünwald–Letnikov scheme, where the history of the internal memory force is used to take account of the damping effect. The classical implicit Newmark predictor-corrector time integration scheme is used to solve the dynamic problem in conjunction with the Newton–Raphson iterative procedure used to solve the non-linear problem. The latter requires the calculation of an internal force vector and a tangent stiffness matrix at each iteration in the time incrementation. The internal force vector is split up such that the term arising from the viscoelastic behavior of the core is shifted to the right-hand side of the equation of motion in order to facilitate the calculations (Galucio et al., 2004). Finally, some examples are presented and analyzed.

2. KINEMATICS

Consider the sandwich beam shown in Figure 1. Euler–Bernoulli hypotheses are assumed for the laminated faces (top and bottom layers), whereas Timoshenko ones are assumed for the core (middle layer). Additionally, all layers are supposed to be perfectly bonded and in plane stress state. The mechanical displacement field for each layer is written as:

$$u_{xi}(x,z,t) = u_i(x,t) - (z - z_i)\theta_i(x,t) \tag{1a}$$

$$u_{zi}(x,z,t) = w(x,t) \tag{1b}$$

where the subscript $i = a, b, c$ stands for upper, lower and middle layers, respectively, u_{xi} and u_{zi} are the axial and transverse displacements of each layer, u_i and θ_i are the axial displacement of the center line and the cross-sectional rotation of each layer and w is the transverse displacement (according to Figure 1 in global coordinate system). Furthermore, in this work, only small strains are considered.

Let us introduce the mean and relative axial displacements given by $\bar{u} = (u_a + u_b)/2$ and $\tilde{u} = u_a - u_b$. Euler–Bernoulli hypotheses for the faces lead to $\theta_k = w'$ for $k = a, b$ with $(\cdot)' = \partial(\cdot)/\partial x$. As all layers are supposed to be perfectly bonded, the displacement continuity conditions at interface layers can be written as $u_{xa} = u_{xc}$ at $z = h_c/2$ and $u_{xb} = u_{xc}$ at $z = -h_c/2$. Therefore, axial displacements of the centerlines and rotations of each layer can be written in terms of w' and the above defined variables $\bar{u}$ and $\tilde{u}$ as:

$$u_a = \bar{u} + \frac{\tilde{u}}{2} \qquad \theta_a = w' \tag{2a}$$

$$u_b = \bar{u} - \frac{\tilde{u}}{2} \qquad \theta_b = w' \tag{2b}$$

$$u_c = \bar{u} + \frac{\tilde{h}}{4} w' \qquad \theta_c = -\frac{\tilde{u} + \bar{h} w'}{h_c} \tag{2c}$$

where $\bar{h}$ and $\tilde{h}$ are defined by $\bar{h} = (h_a + h_b)/2$ and $\tilde{h} = h_a - h_b$.

From Equations (1) and (2), and taking the hypothesis of plane stress state into account, we can write the axial strain of the ith-layer ε_{1i} and the shear strain of the core ε_{5c} as follows ($i = a,\ b,\ c$):

$$\varepsilon_{1i} = \epsilon_i + z\kappa_i, \qquad \varepsilon_{5c} = \gamma_{\,c} \tag{3}$$

where ϵ_i is the membrane strain, κ_i the curvature and $\gamma_{\,c}$ the shear strain of the core. In terms of the above-defined variables, we have:

$$\epsilon_a = \bar{u}' + \frac{\tilde{u}'}{2}, \quad \epsilon_b = \bar{u}' - \frac{\tilde{u}'}{2} \qquad \kappa_a = \kappa_b = -w''$$

$$\epsilon_c = \bar{u}' + \frac{\tilde{h}}{4} w''; \qquad \kappa_c = \frac{\tilde{u}' + \bar{h} w''}{h_c} \qquad \gamma_{\,c} = \frac{\tilde{u}}{h_c} + \left(1 + \frac{\bar{h}}{h_c}\right) w'. \tag{4}$$

Without covering face layers (i.e. $h_a = h_b = 0$), the previous generalized strain quantities of the core correspond to those of a single Timoshenko beam.

3. CONSTITUTIVE EQUATIONS

3.1. Laminated Piezoelectric Faces

The piezoelectric laminated faces are poled in the thickness direction with an electric field applied parallel to this polarization. For the beam case studied in this work, the three-dimensional constitutive equations can be reduced to (with $k = a,\ b$):

$$\begin{aligned} \sigma_{1k} &= \bar{c}^k_{11}\varepsilon_{1k} - \bar{e}^k_{31}E_{3k} \\ D_{3k} &= \bar{e}^k_{31}\varepsilon_{1k} + \bar{d}^k_{33}E_{3k} \end{aligned} \tag{5}$$

where σ_1, ε_1 are the axial stress and strain and D_3, E_3 the transverse electric displacement and field. Modified elastic, piezoelectric and dielectric constants are given by:

$$\bar{c}^k_{11} = c^k_{11} - \frac{(c^k_{13})^2}{c^k_{33}}, \quad \bar{e}^k_{31} = e^k_{31} - \frac{c^k_{13}e^k_{33}}{c^k_{33}}, \quad \bar{d}^k_{33} = d^k_{33} + \frac{(e^k_{33})^2}{c^k_{33}}.$$

For elastic faces, $\bar{e}^k_{31} = 0$ and $\bar{d}^k_{33} = d^k_{33}$. Furthermore, if the material is isotropic $\bar{c}^k_{11} = E/(1-\nu^2)$, where E and ν are the elastic modulus and the Poisson's ratio.

Finally, throughout this work, we assume that the electric potential is linear in the thickness of each piezoelectric layer. This assumption implies a constant transverse electric field:

$$E_{3k} = -V_k/h_k \tag{6}$$

where V_k is the voltage and h_k the thickness of the piezoelectric layer.

3.2. Viscoelastic Core

The one-dimensional constitutive equation introduced by Bagley and Torvik (1983) is adopted in this work to describe the viscoelastic behavior of the core:

$$\sigma + \tau^\alpha \mathcal{D}^\alpha \sigma = E_o\varepsilon + E_\infty \tau^\alpha \mathcal{D}^\alpha \varepsilon \tag{7}$$

where E_o and E_∞ are the relaxed and non-relaxed elastic moduli, τ the relaxation time, α the fractional order of the time derivative ($0 < \alpha < 1$), and D^α denotes the α-derivative operator, which can be approximated by using the Grünwald–Letnikov (GL) power series:

$$\mathcal{D}^\alpha f_n \approx \frac{1}{\Delta t^\alpha}\sum_{j=0}^{N_t} A_{j+1} f_{n-j} \tag{8}$$

where Δt is the time step increment of the numerical scheme, N_t is the truncation number of the series, and A_{j+1} represents the GL-coefficients given either in terms of the gamma function or by a recurrence formula:

$$A_{j+1} = \frac{\Gamma(j-\alpha)}{\Gamma(-\alpha)\Gamma(j+1)} = \frac{j-\alpha-1}{j} A_j. \tag{9}$$

It should be pointed out that the GL-approximation (8) is relatively simple to implement in a finite element code, however two crucial points are not considered in this work. The first one concerns the truncation of the power series. Some strategies have been investigated in recent work, for example, Adolfsson et al. (2004) and Galucio et al. (2004). The second point deals with the accuracy of the scheme used to approximate the fractional differential operator. In this context, recent investigations using other approximations have evaluated their accuracy through theoretical results (Diethelm et al., 2004) and numerical experiments (Galucio et al., 2006).

In order to avoid working with the stress history arising from the approximation of Equation (7), let us introduce the following variable change $\varepsilon^{\mathrm{V}} = \varepsilon - \sigma/E$, such that the constitutive Equation (7) can be rewritten in a discretized form as (Galucio et al., 2004):

$$\varepsilon^{\mathrm{V}}_{n+1} = (1-c_\alpha)\frac{E_\infty - E_o}{E_\infty}\varepsilon_{n+1} - c_\alpha \sum_{j=0}^{N_t} A_{j+1}\varepsilon^{\mathrm{V}}_{n+1-j} \tag{10}$$

where c_α is a dimensionless constant given by $c_\alpha = \dfrac{\tau^\alpha}{\tau^\alpha + \Delta t^\alpha}$.

4. VARIATIONAL FORMULATION

The discrete equations of motion are derived from the Hamilton's principle:

$$\delta \int (T - U + W)\,\mathrm{d}t = 0 \tag{11}$$

where T and U are the kinetic and internal energies and W the external work. For the sake of simplicity, the latter is not detailed here.

In the following, kinetic and internal energies are shown in detail, recalling that inertial and internal force vectors are computed from the variation of these energies. Further, the kinetic energy variation is given by $\delta T = \delta T_a + \delta T_b + \delta T_c$ and the internal energy variation by $\delta U = \delta U_a + \delta U_b + \delta U_c$.

4.1. Variation of the Kinetic Energy

The variation of the kinetic energy of the kth lamina is written as (for $k = a,\ b$)

$$\begin{aligned} \delta T_k &= -\int_{\Omega_k} \rho_k \left(\ddot{u}_{xk}\delta u_{xk} + \ddot{u}_{zk}\delta u_{zk}\right)\mathrm{d}\Omega \\ &= -b\int_0^L \rho_k \left[h_k(\ddot{u}_k\delta u_k + \ddot{w}\delta w) + \frac{h_k^3}{12}\ddot{\theta}_k\delta\theta_k\right]\mathrm{d}x \end{aligned} \tag{12}$$

where an over dot represents differentiation with respect to time, b and L are the width and the total length of the beam, and ρ_k and Ω_k are the mass density and the domain of the kth layer.

The procedure used to compute the kinetic energy of the core is similar to that used for the faces. Then, the variation of the kinetic energy of the core is classically written as

$$\begin{aligned} \delta T_c &= -\int_{\Omega_c} \rho_c \left(\ddot{u}_{xc}\delta u_{xc} + \ddot{u}_{zc}\delta u_{zc}\right) \mathrm{d}\Omega \\ &= -b\int_0^L \rho_c \left[h_c(\ddot{u}_c\delta u_c + \ddot{w}\delta w) + \frac{h_c^3}{12}\ddot{\theta}_c\delta\theta_c\right] \mathrm{d}x \end{aligned} \tag{13}$$

where ρ_c and Ω_c are the mass density and the domain of the core.

4.2. Variation of the Strain Energy

The variation of the internal energy for the piezoelectric laminated faces can be obtained by using Equation (5):

$$\begin{aligned} \delta U_k &= \int_{\Omega_k} (\delta\varepsilon_{1k}\sigma_{1k} - \delta E_{3k}D_{3k})\mathrm{d}\Omega \\ &= \int_{\Omega_k} (\bar{c}_{11}^k\delta\varepsilon_{1k}\varepsilon_{1k} - \bar{e}_{31}^k\delta\varepsilon_{1k}E_{3k} - \bar{e}_{31}^k\delta E_{3k}\varepsilon_{1k} - \bar{d}_{33}^k\delta E_{3k}E_{3k})\mathrm{d}\Omega \\ &= \delta U_k^{\mathrm{M}} + \delta U_k^{\mathrm{ME}} + \delta U_k^{\mathrm{EM}} + \delta U_k^{\mathrm{E}} \end{aligned} \tag{14}$$

where $k = a, b$ and superscripts M, ME, EM and E stand for mechanical, piezoelectric and dielectric contributions. These terms can be obtained using Equations (3) and (6):

$$\delta U_k^{\mathrm{M}} = \int_0^L \bar{c}_{11}^k(A_k\delta\epsilon_k\epsilon_k + I_k\delta\kappa_k\kappa_k)\mathrm{d}x \tag{15a}$$

$$\delta U_k^{\mathrm{ME}} = \int_0^L \bar{e}_{31}^k\frac{A_k}{h_k}\delta\epsilon_k V_k\mathrm{d}x \tag{15b}$$

$$\delta U_k^{\mathrm{EM}} = \int_0^L \bar{e}_{31}^k\frac{A_k}{h_k}\delta V_k\epsilon_k\mathrm{d}x \tag{15c}$$

$$\delta U_k^{\mathrm{E}} = -\int_0^L \bar{d}_{33}^k\frac{A_k}{h_k^2}\delta V_k V_k\mathrm{d}x \tag{15d}$$

where A_k is the cross-sectional area and I_k the moment of inertia of each laminated layer.

Using Equations (7) and (10), the variation of the internal energy of the viscoelastic core is given by

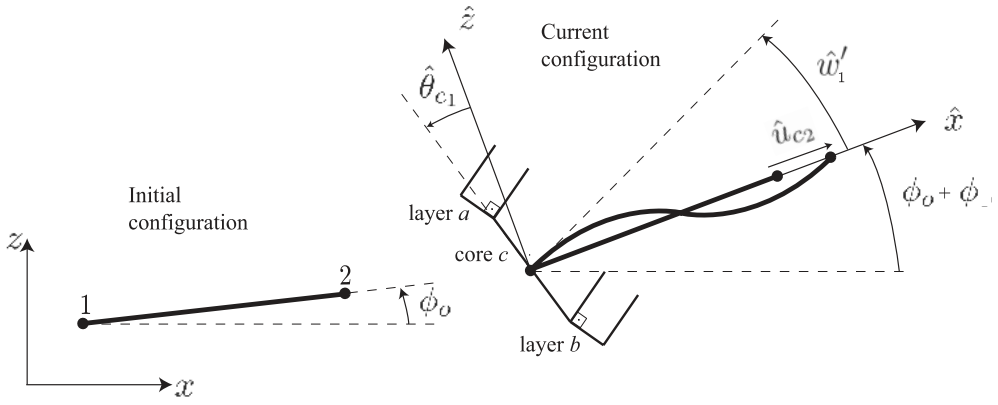

Figure 2. Co-rotational configuration of sandwich beam.

$$
\begin{aligned}
\delta U_c &= \int_{\Omega_c} (\delta\varepsilon_{1c}\sigma_{1c} + \delta\varepsilon_{5c}\sigma_{5c})\mathrm{d}\Omega \\
&= (1+c_v)\int_{\Omega_c} \left[\bar{c}^c_{11}\delta\varepsilon_{1c}\varepsilon_{1c} + \bar{c}^c_{55}\delta\varepsilon_{5c}\varepsilon_{5c}\right]\mathrm{d}\Omega \\
&+ (c_\alpha + c_v)\sum_{j=1}^{N_t} A_{j+1}\int_{\Omega_c} \left[\bar{c}^c_{11}\delta\varepsilon_{1c}(\varepsilon^{\mathrm{V}}_{1c})^{n+1-j} + \bar{c}^c_{55}\delta\varepsilon_{5c}(\varepsilon^{\mathrm{V}}_{5c})^{n+1-j}\right]\mathrm{d}\Omega \\
&= (1+c_v)\,\delta U^{\mathrm{M}}_c + (c_\alpha + c_v)\delta U^{\mathrm{V}}_c \qquad (16)
\end{aligned}
$$

where $c_v = c_\alpha(E \quad - E_o)/E_o$, $\bar{c}^c_{11} = E_o/(1-\nu^2)$ and $\bar{c}^c_{55} = E_o/(2+2\nu)$. The superscript V stands for viscoelastic contribution.

Note that the second term in Equation (16) depends on the history of ε^{V}. In order to facilitate the numerical integration, once discretized, this term is treated as an external dissipative force (see Section 5.7).

5. CO-ROTATIONAL FORMULATION

5.1. Sandwich Beam Model

Consider the sandwich beam element shown in Figure 2. This beam element allows large displacements and rotations within the context of small strains. Recall that in a co-rotational element, the rigid body motion is dissociated from elastic deformations. Therefore, a local mobile frame, which is related to a rigid body motion of each element, is used to measure the strains while the internal force vector and the tangent stiffness matrix are evaluated in the inertial frame. This allows solution of the dynamic equations in the global coordinate system. For a thorough review of corotational finite elements, the reader is referred to the didactic work proposed by Felippa and Haugen (2005).

Figure 2 shows the initial configuration associated to angle ϕ_o (global-coordinate system) and the current configuration after a rigid body rotation ϕ (local-coordinate system). In the initial configuration, the position of nodes 1 and 2 is defined in the global coordinate system by $(x_1,\ z_1)$ and $(x_2,\ z_2)$ (same as in Section 2). The current configuration is associated to the mobile frame $(x_\cdot\ ,\ z_\cdot)$, such that its origin is placed on the node 1 and the $x_\cdot$-axis passes through node 2. Moreover, the notation $(\bullet)$ is related to entities in the local frame.

In order to derive the co-rotational formulation, a set of local degrees-of-freedom is chosen. These variables are associated to axial displacement (u_c), cross-sectional rotation ($\hat{\theta}_c$) and derivative of the transverse displacement ($\hat{w}'$). They are written in terms of the global degrees-of-freedom by:

$$\begin{array}{lllll} \text{Node 1:} & \hat{u}_{c_1} = 0 & \hat{w}'_1 = \beta_1 - \phi & \hat{\theta}_{c_1} = \theta_{c_1} - \phi \\ \text{Node 2:} & \hat{u}_{c_2} = \ell - \ell_o & \hat{w}'_2 = \beta_2 - \phi & \hat{\theta}_{c_2} = \theta_{c_2} - \phi \end{array} \tag{17}$$

where ℓ_o and ℓ are the initial and current length of the element, defined in the global coordinate system as:

$$\ell_o = \sqrt{x_{21}^2 + z_{21}^2} \tag{18}$$

$$\ell = \sqrt{(x_{21} + u_{c_{21}})^2 + (z_{21} + w_{21})^2} \tag{19}$$

with $(\bullet)_{21} = (\bullet)_2 - (\bullet)_1$.

It should be emphasized that these local variables behave alike the global ones. Then, similarly to Equation (2c), the mean and relative axial displacements in the local frame are given by:

$$\hat{\bar{u}}_i = \hat{u}_{c_i} - \frac{\tilde{h}}{4}\hat{w}'_i \qquad \hat{\tilde{u}}_i = -h_c\hat{\theta}_{c_i} - \bar{h}\hat{w}'_i \tag{20}$$

where the subscript i stands for the position of the node, such that $i = 1,\ 2$.

Let us introduce the local degrees-of-freedom vector:

$$\hat{\mathbf{q}} = [\hat{\bar{u}}_1 \quad \hat{w}'_1 \quad \hat{\tilde{u}}_1 \quad \hat{\bar{u}}_2 \quad \hat{w}'_2 \quad \hat{\tilde{u}}_2 \quad \hat{V}_a \quad \hat{V}_b]^{\mathrm{T}} \tag{21}$$

and the global one:

$$\mathbf{q} = [\bar{u}_1 \quad w_1 \quad \beta_1 \quad \tilde{u}_1 \quad \bar{u}_2 \quad w_2 \quad \beta_2 \quad \tilde{u}_2 \quad V_a \quad V_b]^{\mathrm{T}}. \tag{22}$$

Note that both vectors are composed of mechanical and electrical degrees-of-freedom. The latter is the voltage in the piezoelectric layer such that $\hat{V}_a = V_a$ and $\hat{V}_b = V_b$.

Using Equations (17) and (20), the mechanical variables of $\hat{\mathbf{q}}$ can be written in terms of the components of $\mathbf{q}$ as:

$$\begin{aligned} \hat{\tilde{u}}_1 &= -h_1(\beta_1 - \phi) & \hat{w}'_1 &= \beta_1 - \phi & \hat{\tilde{u}}_1 &= \tilde{u}_1 + h_2\phi \\ \hat{\tilde{u}}_2 &= \ell - \ell_o - h_1(\beta_2 - \phi) & \hat{w}'_2 &= \beta_2 - \phi & \hat{\tilde{u}}_2 &= \tilde{u}_2 + h_2\phi \end{aligned} \tag{23}$$

where $h_1 = \dfrac{\tilde{h}}{4}$ and $h_2 = h_c + \bar{h}$.

In order to write the trigonometric functions of ϕ in terms of global variables, we use:

$$\cos\phi = c_o c + s_o s \qquad \sin\phi = c_o s - s_o c \tag{24}$$

with:

$$c_o = \cos\phi_o = \frac{x_{21}}{\ell_o} \qquad s_o = \sin\phi_o = \frac{z_{21}}{\ell_o} \tag{25a}$$

$$c = \cos(\phi_o + \phi) = \frac{x_{21} + u_{c_{21}}}{\ell} \qquad s = \sin(\phi_o + \phi) = \frac{z_{21} + w_{21}}{\ell}. \tag{25b}$$

5.2. Virtual Local Displacements

The goal of this section is to write a relation between the virtual local displacement vector $\delta\hat{\mathbf{q}}$ and the virtual global displacement vector $\delta\mathbf{q}$. This implies calculating the variation of Equation (23):

$$\begin{aligned} \delta\hat{\tilde{u}}_1 &= -h_1(\delta\beta_1 - \delta\phi) & \delta\hat{w}'_1 &= \delta\beta_1 - \delta\phi & \delta\tilde{\bar{u}}_1 &= \delta\tilde{u}_1 + h_2\delta\phi \\ \delta\hat{\tilde{u}}_2 &= \delta\ell - h_1(\delta\beta_2 - \delta\phi) & \delta\hat{w}'_2 &= \delta\beta_2 - \delta\phi & \delta\tilde{\bar{u}}_2 &= \delta\tilde{u}_2 + h_2\delta\phi \end{aligned} \tag{26}$$

where two variations must be calculated: $\delta\ell$ and $\delta\phi$. The virtual current length of the sandwich beam, which is derived from Equation (19), is defined as:

$$\delta\ell = c\delta u_{c_{21}} + s\delta w_{21} = c\delta\bar{u}_{21} + s\delta w_{21} + h_1 c\delta\beta_{21} \tag{27}$$

or in terms of the virtual global displacement vector:

$$\delta\ell = \mathbf{r}^{\mathrm{T}}\delta\mathbf{q} \tag{28}$$

where the vector $\mathbf{r}$ is defined by:

$$\mathbf{r} = \begin{bmatrix} -c & -s & -h_1 c & 0 & c & s & h_1 c & 0 & 0 & 0 \end{bmatrix}^{\mathrm{T}}. \tag{29}$$

Concerning $\delta\phi$, let us write the variation of the sinus expression in Equation (25b) as:

$$\delta s = c\,\delta\phi = \frac{\ell\delta w_{21} - (z_{21} + w_{21})\delta\ell}{\ell^2}. \tag{30}$$

Substituting Equation (27) into Equation (30), the variation of ϕ can be then written in terms of global variables as:

$$\delta\phi = -\frac{s}{\ell}\delta u_{c_{21}} + \frac{c}{\ell}\delta w_{21} = -\frac{s}{\ell}\delta\bar{u}_{21} + \frac{c}{\ell}\delta w_{21} - \frac{h_1 s}{\ell}\delta\beta_{21} \tag{31}$$

or in terms of the virtual global displacement vector:

$$\delta\phi = \frac{1}{\ell}\mathbf{z}^{\mathrm{T}}\delta\mathbf{q} \tag{32}$$

with

$$\mathbf{z} = \begin{bmatrix} s & -c & h_1 s & 0 & -s & c & -h_1 s & 0 & 0 & 0 \end{bmatrix}^{\mathrm{T}}. \tag{33}$$

Substituting Equation (32) into Equation (26), one obtains the relation between $\delta\hat{\mathbf{q}}$ and $\delta\mathbf{q}$, i.e.

$$\delta\hat{\mathbf{q}} = \mathbf{T}\delta\mathbf{q} \tag{34}$$

where $\mathbf{T}$ is the transformation matrix whose components are given in Appendix A.

5.3. Finite Element Discretization

The aim of this subsection is to provide a spatial discretization of the variational formulation outlined in Section 4 by using classical techniques.

Linear and cubic shape functions are used to approximate axial displacements and deflections in the local coordinate system. They are:

$$H_1 = 1 - \frac{x}{\ell_o} \tag{35a}$$

$$H_2 = \frac{x}{\ell_o} \tag{35b}$$

$$H_3 = x\left(1 - \frac{x}{\ell_o}\right)^2 \tag{35c}$$

$$H_4 = -\frac{x^2}{\ell_o}\left(1 - \frac{x}{\ell_o}\right) \tag{35d}$$

where x is the axial position and ℓ_o the initial length of the beam.

Using Equations (35), strains and voltages as well their variations can be approximated by:

$$\begin{array}{cccc} \epsilon_i = \mathbf{B}_{mi}\hat{\mathbf{q}}, & \kappa_i = \mathbf{B}_{bi}\hat{\mathbf{q}}, & \gamma_c = \mathbf{B}_{sc}\hat{\mathbf{q}}, & \hat{V}_k = \mathbf{H}_{vk}\hat{\mathbf{q}} \\ \delta\epsilon_i = \delta\hat{\mathbf{q}}^{\mathrm{T}}\mathbf{B}_{mi}^{\mathrm{T}}, & \delta\kappa_i = \delta\hat{\mathbf{q}}^{\mathrm{T}}\mathbf{B}_{bi}^{\mathrm{T}}, & \delta\gamma_c = \delta\hat{\mathbf{q}}^{\mathrm{T}}\mathbf{B}_{sc}^{\mathrm{T}}, & \delta\hat{V}_k = \delta\hat{\mathbf{q}}^{\mathrm{T}}\mathbf{H}_{vk}^{\mathrm{T}} \end{array} \tag{36}$$

where the following subscripts are used: i stands for the layer $i = a, b, c$; k for faces, i.e. $k = a, b$; m for membrane strain; b for bending strain; and s for shear strain. Addition-

ally, the displacement-strain matrix operators $\mathbf{B}$ associated to membrane, bending and shear strains are defined as:

$$\mathbf{B}_{mi} = \mathbf{H}'_{xi}, \quad \mathbf{B}_{bi} = \mathbf{H}'_{ri} \quad \text{and} \quad \mathbf{B}_{sc} = \mathbf{H}_{rc} - \mathbf{H}_{rk} \tag{37}$$

with the interpolation vectors related to axial displacements $\mathbf{H}_x$, rotations $\mathbf{H}_r$ and voltages $\mathbf{H}_v$ given by:

$$\mathbf{H}_{xa} = [\ H_1 \quad 0 \quad H_1/2 \quad H_2 \quad 0 \quad H_2/2 \quad 0 \quad 0\ ] \tag{38a}$$

$$\mathbf{H}_{xb} = [\ H_1 \quad 0 \quad -H_1/2 \quad H_2 \quad 0 \quad -H_2/2 \quad 0 \quad 0\ ] \tag{38b}$$

$$\mathbf{H}_{xc} = [\ H_1 \quad h_1 H'_3 \quad 0 \quad H_2 \quad h_1 H'_4 \quad 0 \quad 0 \quad 0\ ] \tag{38c}$$

$$\mathbf{H}_{rk} = [\ 0 \quad -H'_3 \quad 0 \quad 0 \quad -H'_4 \quad 0 \quad 0 \quad 0\ ] \tag{38d}$$

$$\mathbf{H}_{rc} = [\ 0 \quad (h_2/h_c - 1)H'_3 \quad H_1/h_c \quad 0 \quad (h_2/h_c - 1)H'_4 \quad H_2/h_c \quad 0 \quad 0\ ] \tag{38e}$$

$$\mathbf{H}_{va} = [\ 0 \quad 0 \quad 0 \quad 0 \quad 0 \quad 0 \quad 1 \quad 0\ ] \tag{38f}$$

$$\mathbf{H}_{vb} = [\ 0 \quad 0 \quad 0 \quad 0 \quad 0 \quad 0 \quad 0 \quad 1\ ]. \tag{38g}$$

5.4. Mass Matrix

The mass matrix of the sandwich beam is derived from the finite element discretization of Equations (12) and (13). Hence, the elementary mass matrices of each piezoelectric face ($k = a,\ b$), arising from the discretization of Equation (12), is given by:

$$\mathbf{M}_k = \int_0^{\ell_o} \rho_k \left[A_k \left(\mathbf{H}_{xk}^{\mathrm{T}} \mathbf{H}_{xk} + \mathbf{H}_z^{\mathrm{T}} \mathbf{H}_z \right) + I_k \mathbf{H}_{rk}^{\mathrm{T}} \mathbf{H}_{rk} \right] \mathrm{d}x \tag{39}$$

and that of the core, arising from the discretization of Equation (13), is classically defined as:

$$\mathbf{M}_c = \int_0^{\ell_o} \rho_c \left[A_c \left(\mathbf{H}_{xc}^{\mathrm{T}} \mathbf{H}_{xc} + \mathbf{H}_z^{\mathrm{T}} \mathbf{H}_z \right) + I_c \mathbf{H}_{rc}^{\mathrm{T}} \mathbf{H}_{rc} \right] \mathrm{d}x. \tag{40}$$

It should be stressed that the electromechanical coupling within piezoelectric faces and the viscoelastic behavior of the core are not involved in the calculation of the mass matrix. These piezoelectric and viscoelastic contributions are taken into account through the internal force vector and/or external forces as described below.

5.5. Internal Force Vectors

Using expressions (15) and (16), the internal force vectors are obtained through the relation:

$$\delta U = \delta \mathbf{q}^{\mathrm{T}} \mathbf{F} = \delta \hat{\mathbf{q}}^{\mathrm{T}} \hat{\mathbf{F}} = \delta \mathbf{q}^{\mathrm{T}} \mathbf{T}^{\mathrm{T}} \hat{\mathbf{F}} \tag{41}$$

where $\mathbf{F}$ is the global internal force vector and $\hat{\mathbf{F}}$ the local internal force vector.

It should be noted that Equation (41) must hold for all $\delta\mathbf{q}$, therefore the internal force vector, written in the global coordinate system, is given by:

$$\mathbf{F} = \mathbf{T}^{\mathrm{T}}\hat{\mathbf{F}} \tag{42}$$

with the local internal force vector defined as:

$$\hat{\mathbf{F}} = \sum_{k=a,b} (\hat{\mathbf{F}}_k^{\mathrm{M}} + \hat{\mathbf{F}}_k^{\mathrm{ME}} + \hat{\mathbf{F}}_k^{\mathrm{EM}} + \hat{\mathbf{F}}_k^{\mathrm{E}}) + (1 + c_v)\hat{\mathbf{F}}_c^{\mathrm{M}} \tag{43}$$

where $\hat{\mathbf{F}}_i^{\mathrm{M}}$ (with $i = a, b, c$) is the mechanical internal force vector; $\hat{\mathbf{F}}_k^{\mathrm{ME}}$ and $\hat{\mathbf{F}}_k^{\mathrm{EM}}$ the piezoelectric internal force vector; $\hat{\mathbf{F}}_k^{\mathrm{E}}$ the dielectric internal force vector; and $c_v\hat{\mathbf{F}}_c^{\mathrm{M}}$ the added-mechanical internal force vector associated to the viscoelastic behavior of the core. For illustrative purposes, these vectors are given in the Appendix B.

Another way of writing the local internal force vector deals with the concept of generalized forces such that:

$$\hat{\mathbf{F}} = \begin{bmatrix} \bar{N}_1 & M_1 & \tilde{N}_1 & \bar{N}_2 & M_2 & \tilde{N}_2 & Q_a & Q_b \end{bmatrix}^{\mathrm{T}} \tag{44}$$

where each component is associated to those of the local degree-of-freedom vector defined in Equation (21). It is worth mentioning that this way of writing $\hat{\mathbf{F}}$ is useful for the calculation of the geometric stiffness matrix as we shall see below.

5.6. Tangent Stiffness Matrix

The global tangent stiffness matrix $\mathbf{K}_{\mathrm{T}}$ is derived by differentiating the internal force vector through the degree-of-freedom vector, i.e.:

$$\delta\mathbf{F} = \mathbf{K}_{\mathrm{T}}\delta\mathbf{q}. \tag{45}$$

This relation can be rewritten by using Equation (42):

$$\delta\mathbf{F} = \mathbf{T}^{\mathrm{T}}\delta\hat{\mathbf{F}} + \delta\mathbf{T}^{\mathrm{T}}\hat{\mathbf{F}} = \mathbf{K}_{\mathrm{M}}\delta\mathbf{q} + \mathbf{K}_{\mathrm{G}}\delta\mathbf{q} \tag{46}$$

where $\mathbf{K}_{\mathrm{M}}$ and $\mathbf{K}_{\mathrm{G}}$ are the material and geometric stiffness matrices, such that

$$\mathbf{K}_{\mathrm{T}} = \mathbf{K}_{\mathrm{M}} + \mathbf{K}_{\mathrm{G}}. \tag{47}$$

The calculation of these matrices is carried out below noting that, cf. Equation (46), $\mathbf{K}_{\mathrm{M}}$ depends on the variation of the internal force vector while $\mathbf{K}_{\mathrm{G}}$ depends on the variation of the transformation matrix.

5.6.1. Material stiffness matrix

Following Equation (46), the calculation of $\mathbf{K}_{\mathrm{M}}$ is related to:

$$\mathbf{K}_{\mathrm{M}}\delta\mathbf{q} = \mathbf{T}^{\mathrm{T}}\delta\hat{\mathbf{F}} \tag{48}$$

where $\mathbf{T}$ is given in Appendix A. Concerning the calculation of $\delta\hat{\mathbf{F}}$, let us introduce a local (8×8)-matrix such that:

$$\delta\hat{\mathbf{F}} = \hat{\mathbf{K}}\delta\hat{\mathbf{q}} \tag{49}$$

where the components of $\hat{\mathbf{K}}$ are given in Appendix C.

By combining Equations (34), (48) and (49), the material stiffness matrix written in global coordinate system is given by:

$$\mathbf{K}_{\mathrm{M}} = \mathbf{T}^{\mathrm{T}}\hat{\mathbf{K}}\mathbf{T}. \tag{50}$$

Noting that $\mathbf{K}_{\mathrm{M}}$ is a (10×10)-matrix written in the global coordinate system.

5.6.2. Geometric stiffness matrix

As above mentioned, the geometric stiffness matrix is obtained from the expression:

$$\mathbf{K}_{\mathrm{G}}\delta\mathbf{q} = \delta\mathbf{T}^{\mathrm{T}}\hat{\mathbf{F}} \tag{51}$$

which requires the calculation of $\delta\mathbf{T}$. For this purpose, let us rewrite the right-hand side of Equation (51) using Equation (44):

$$\delta\mathbf{T}^{\mathrm{T}}\hat{\mathbf{F}} = \bar{N}_1\delta\mathbf{T}_1 + M_1\delta\mathbf{T}_2 + \tilde{N}_1\delta\mathbf{T}_3 + \bar{N}_2\delta\mathbf{T}_4 + M_2\delta\mathbf{T}_5 + \tilde{N}_2\delta\mathbf{T}_6 + Q_a\delta\mathbf{T}_7 + Q_b\delta\mathbf{T}_8 \tag{52}$$

where each (1×8)-vector $\mathbf{T}_i$ $(i = 1, \ldots, 8)$ represents the ith row of $\mathbf{T}$, defined in Equation (76), Appendix A. Consistent with Equation (77), the variation of $\mathbf{T}$ depends on $\delta\ell$, $\delta\mathbf{r}$ and $\delta\mathbf{z}$:

$$\begin{bmatrix} \delta\mathbf{T}_1 \\ \delta\mathbf{T}_2 \\ \delta\mathbf{T}_3 \\ \delta\mathbf{T}_4 \\ \delta\mathbf{T}_5 \\ \delta\mathbf{T}_6 \\ \delta\mathbf{T}_7 \\ \delta\mathbf{T}_8 \end{bmatrix} = -\frac{1}{\ell^2}\begin{bmatrix} h_1 \\ -1 \\ h_2 \\ h_1 \\ -1 \\ h_2 \\ 0 \\ 0 \end{bmatrix}(\ell\delta\mathbf{z}^{\mathrm{T}} - \mathbf{z}^{\mathrm{T}}\delta\ell) + \begin{bmatrix} 0 \\ 0 \\ 0 \\ 1 \\ 0 \\ 0 \\ 0 \\ 0 \end{bmatrix}\delta\mathbf{r}. \tag{53}$$

Noting that $\delta\mathbf{r} = \mathbf{z}\delta\phi = \frac{1}{\ell}\mathbf{z}\mathbf{z}^{\mathrm{T}}\delta\mathbf{q}$ and $\delta\mathbf{z} = -\mathbf{r}\delta\phi = -\frac{1}{\ell}\mathbf{r}\mathbf{z}^{\mathrm{T}}\delta\mathbf{q}$. In addition, $\delta\ell$ and $\delta\phi$ are given by Equations (28) and (32), respectively. Using these relations, the transpose of $\delta\mathbf{T}$ is then:

$$\begin{aligned}\delta\mathbf{T}^{\mathrm{T}} &= -\frac{1}{\ell^2}(\mathbf{r}\mathbf{z}^{\mathrm{T}} + \mathbf{z}\mathbf{r}^{\mathrm{T}})\delta\mathbf{q}[\ h_1 \quad -1 \quad h_2 \quad h_1 \quad -1 \quad h_2 \quad 0 \quad 0\ ] \\ &+ \frac{1}{\ell}\mathbf{z}\mathbf{z}^{\mathrm{T}}\delta\mathbf{q}[\ 0 \quad 0 \quad 0 \quad 1 \quad 0 \quad 0 \quad 0 \quad 0\ ]. \end{aligned} \tag{54}$$

The substitution of Equation (54) into (52) provides the geometric stiffness matrix:

$$\mathbf{K}_{\mathrm{G}} = \frac{1}{\ell}\bar{N}_2\mathbf{z}\mathbf{z}^{\mathrm{T}} - \frac{1}{\ell^2}\left[h_1(\bar{N}_1 + \bar{N}_2) - (M_1 + M_2) + h_2(\tilde{N}_1 + \tilde{N}_2)\right](\mathbf{r}\mathbf{z}^{\mathrm{T}} + \mathbf{z}\mathbf{r}^{\mathrm{T}}) \tag{55}$$

where $\mathbf{K}_{\mathrm{G}}$ is a (10×10)-matrix written in the global coordinate system.

5.7. Complete and Reduced System

Recall that we are seeking to solve a problem in non-linear dynamics in which several parameters are involved, i.e. to control a sandwich beam with viscoelastic core and piezoelectric/elastic laminated faces undergoing large displacements and rotations. In order to take the electromechanical coupling into account, electrical degrees-of-freedom are used in the formulation, in concordance with the global degree-of-freedom vector defined in Equation (22). This vector can be rewritten as:

$$\mathbf{q} = [\mathbf{q}^{\mathrm{M}} \quad \mathbf{V}]^{\mathrm{T}} \tag{56}$$

where $\mathbf{q}^{\mathrm{M}}$ represents the mechanical global degree-of-freedom vector (first eight lines of $\mathbf{q}$) and $\mathbf{V}$ the voltage vector such that $\mathbf{V} = [V_a \quad V_b]^{\mathrm{T}}$. Using this notation, the non-linear problem to be solved in the inertial frame is described as:

$$\begin{aligned}&\begin{bmatrix} \mathbf{M} & \mathbf{0} \\ \mathbf{0} & \mathbf{0} \end{bmatrix}\begin{bmatrix} \ddot{\mathbf{q}}^{\mathrm{M}}_{n+1} \\ \ddot{\mathbf{V}}_{n+1} \end{bmatrix} + \begin{bmatrix} \mathbf{F}^{\mathrm{M}}(\mathbf{q}_{n+1}) + c_v\mathbf{F}^{\mathrm{M}}_{c}(\mathbf{q}_{n+1}) + \mathbf{F}^{\mathrm{ME}}(\mathbf{q}_{n+1}) \\ \mathbf{F}^{\mathrm{EM}}(\mathbf{q}_{n+1}) + \mathbf{F}^{\mathrm{E}}(\mathbf{q}_{n+1}) \end{bmatrix} \\ &= \begin{bmatrix} \mathbf{G}^{\mathrm{M}}_{n+1} + \mathbf{G}^{\mathrm{V}}_{n+1} \\ \mathbf{0} \end{bmatrix} \end{aligned} \tag{57}$$

where $\mathbf{M}$ is the global mass matrix such that $\mathbf{M} = \mathbf{M}_a + \mathbf{M}_b + \mathbf{M}_c$, noting that $\mathbf{M}_a$ and $\mathbf{M}_b$ are defined in Equation (39) and $\mathbf{M}_c$ in Equation (40). It should be underlined that the total mass matrix is singular due to the non-inertial electrical degrees-of-freedom. In order to overcome such a difficulty, an elimination of the electrical degrees-of-freedom can be performed at elementary level as we shall see later.

The second term in the left-hand side of Equation (57) represents the internal force vectors, which are thoroughly described in Appendix B. Thus, in the first line, the mechanical contribution is given in Equation (78) and the electromechanical one in Equation (82). In the

second line, we find the electromechanical contribution and the dielectric one both defined in Equations (83) and (84), respectively.

In the right-hand side of Equation (57), two external force vectors appear. They are related to a classical time-dependent mechanical load $\mathbf{G}^{\mathrm{M}}$ and a dissipative load $\mathbf{G}^{\mathrm{V}}$ arising from the viscoelastic constitutive law of the core. The latter is derived from the discretization of the second term of Equation (16), i.e.

$$\mathbf{G}^{\mathrm{V}}_{n+1} = -(c_\alpha + c_v) \sum_{j=1}^{N_t} A_{j+1} \mathbf{F}^{\mathrm{V}}(\mathbf{q}_{n+1-j}). \tag{58}$$

The minus sign is due to the shifting of this term from internal energy to external dissipative one, as mentioned in the end of Section 4. The internal force vector associated to the "anelastic" strain is represented by $\mathbf{F}^{\mathrm{V}}$, which depends on the history of the degree-of-freedom vector. Such a vector is called here internal memory force vector, which is computed by discretizing Equation (10):

$$\mathbf{F}^{\mathrm{V}}(\mathbf{q}_{n+1}) = (1 - c_\alpha) \frac{E_\infty - E_o}{E_\infty} \mathbf{F}^{\mathrm{M}}_c(\mathbf{q}_{n+1}) - c_\alpha \sum_{j=1}^{N_t} A_{j+1} \mathbf{F}^{\mathrm{V}}(\mathbf{q}_{n+1-j}) \tag{59}$$

where the mechanical internal force vector $\mathbf{F}^{\mathrm{M}}_c$ associated to the core is defined by Equation (80).

It might be worthwhile considering the elastic case for which $c_\alpha = 0$ and consequently $c_v = 0$. This implies the terms $c_v \mathbf{F}^{\mathrm{M}}_c$ and $\mathbf{G}^{\mathrm{V}}$, appearing in Equation (57), vanish.

5.7.1. Reduced-order System

Let us split up the displacement vector in mechanical $\mathbf{q}^{\mathrm{M}}$ and electrical sensor/actuator parts (V^{S} and V^{A}) as:

$$\mathbf{q} = [\mathbf{q}^{\mathrm{M}} \quad V^{\mathrm{S}} \quad V^{\mathrm{A}}]^{\mathrm{T}}. \tag{60}$$

According to this notation, the system described in Equation (57) becomes:

$$\begin{bmatrix} \mathbf{M} & \mathbf{0} & \mathbf{0} \\ \mathbf{0} & \mathbf{0} & \mathbf{0} \\ \mathbf{0} & \mathbf{0} & \mathbf{0} \end{bmatrix} \begin{bmatrix} \ddot{\mathbf{q}}^{\mathrm{M}}_{n+1} \\ \ddot{V}^{\mathrm{S}}_{n+1} \\ \ddot{V}^{\mathrm{A}}_{n+1} \end{bmatrix} + \begin{bmatrix} \mathbf{F}^{\mathrm{M}}(\mathbf{q}_{n+1}) + c_v \mathbf{F}^{\mathrm{M}}_c(\mathbf{q}_{n+1}) \\ \mathbf{0} \\ \mathbf{0} \end{bmatrix} + \begin{bmatrix} \mathbf{F}^{\mathrm{ME}}_{\mathrm{S}}(\mathbf{q}_{n+1}) \\ \mathbf{0} \\ \mathbf{0} \end{bmatrix}$$
$$+ \begin{bmatrix} \mathbf{0} \\ \mathbf{F}^{\mathrm{EM}}_{\mathrm{S}}(\mathbf{q}_{n+1}) \\ \mathbf{F}^{\mathrm{EM}}_{\mathrm{A}}(\mathbf{q}_{n+1}) \end{bmatrix} + \begin{bmatrix} \mathbf{0} \\ \mathbf{F}^{\mathrm{E}}_{\mathrm{S}}(\mathbf{q}_{n+1}) \\ \mathbf{F}^{\mathrm{E}}_{\mathrm{A}}(\mathbf{q}_{n+1}) \end{bmatrix} = \begin{bmatrix} \mathbf{G}^{\mathrm{M}}_{n+1} + \mathbf{G}^{\mathrm{V}}_{n+1} + \mathbf{G}^{\mathrm{ME}}_{n+1} \\ \mathbf{0} \\ \mathbf{0} \end{bmatrix} \tag{61}$$

where the local components of the piezoelectric and dielectric internal force vectors are defined in Appendix B. Furthermore, a new vector appears in the right-hand side of this equation. It deals with the piezoelectric internal force vector associated to an actuator configuration. Indeed, in the first line of the system, an added-internal force vector associated to a sensor configuration $\mathbf{F}_{\mathrm{S}}^{\mathrm{ME}}$ appears in the left-hand side and an electric force $\mathbf{G}^{\mathrm{ME}}$ in the right-hand side. The latter is related to the piezoelectric internal force vector by:

$$\mathbf{G}^{\mathrm{ME}} = -\mathbf{F}_{\mathrm{A}}^{\mathrm{ME}} \tag{62}$$

where, for each layer, we have in the global coordinates system:

$$\mathbf{G}_a^{\mathrm{ME}} = -\bar{e}_{31}^a \frac{A_a}{h_a} V^{\mathrm{A}} \mathbf{g}_a \tag{63a}$$

$$\mathbf{G}_b^{\mathrm{ME}} = -\bar{e}_{31}^b \frac{A_b}{h_b} V^{\mathrm{A}} \mathbf{g}_b \tag{63b}$$

with the corresponding vectors:

$$\mathbf{g}_a = \begin{bmatrix} -c & -s & (1-c)h_1 & -1/2 & c & s & -(1-c)h_1 & 1/2 \end{bmatrix}^{\mathrm{T}} \tag{64a}$$

$$\mathbf{g}_b = \begin{bmatrix} -c & -s & (1-c)h_1 & 1/2 & c & s & -(1-c)h_1 & -1/2 \end{bmatrix}^{\mathrm{T}}. \tag{64b}$$

Note that V^{A} is the voltage applied to the piezoelectric layer, a known variable in the problem. Moreover, we assume that the piezoelectric sensor/actuator is associated with only one laminated face (a or b), not with both.

When effecting the elimination of the electrical degrees-of-freedom in the system (61), the third line is automatically verified. The second line, which is represented by:

$$\mathbf{F}_{\mathrm{S}}^{\mathrm{EM}}(\mathbf{q}_{n+1}) + \mathbf{F}_{\mathrm{S}}^{\mathrm{E}}(\mathbf{q}_{n+1}) = \mathbf{0} \tag{65}$$

gives the measured voltage in the piezoelectric sensor in terms of the local displacements:

$$V_a^{\mathrm{S}} = \frac{\bar{e}_{31}^a}{\bar{d}_{33}^a} \frac{h_a}{\ell_o} \left(\hat{\hat{u}}_{21} + \frac{\hat{\hat{u}}_{21}}{2} \right) \tag{66a}$$

$$V_b^{\mathrm{S}} = \frac{\bar{e}_{31}^b}{\bar{d}_{33}^b} \frac{h_b}{\ell_o} \left(\hat{\hat{u}}_{21} - \frac{\hat{\hat{u}}_{21}}{2} \right). \tag{66b}$$

In the first line of Equation (61), we note an added internal force vector associated to a sensor configuration $\mathbf{F}_{\mathrm{S}}^{\mathrm{ME}}$. This vector depends on the measured voltage V^{S} as:

$$\mathbf{F}_{\mathrm{S}a}^{\mathrm{ME}} = \bar{e}_{31}^a \frac{A_a}{h_a} V^{\mathrm{S}} \mathbf{g}_a \tag{67a}$$

$$\mathbf{F}_{\mathrm{S}b}^{\mathrm{ME}} = \bar{e}_{31}^b \frac{A_b}{h_b} V^{\mathrm{S}} \mathbf{g}_b \tag{67b}$$

Table 1. Newmark (average acceleration) / Newton-Raphson algorithm.

1. Enter time step loop
   $t_{n+1} = t_n + \Delta t$
2. Predict displacement, velocity and acceleration: Equation (69)
3. Calculate the dissipative load: Equation (58)
4. Evaluate residual: Equation (70)
5. Convergence analysis

   5Y. If $\| \mathbf{R}_{n+1} \| < \varepsilon$ is true
   - a) Update $\mathbf{F}^{\mathrm{V}}$: Equation (59)

   5N. Else
   - a) Calculate the iteration matrix: Equation (71)
   - b) Calculate the correction: Equation (72)
   - c) Correct the solution: Equation (73)
   - d) Control law
     - Evaluate the sensor voltage: Equation (66)
     - Compute $\mathbf{F}_{\mathrm{S}}^{\mathrm{ME}}$: Equation (67)
     - Calculate the time derivative of V^{S}: Equation (75)
     - Compute the actuator voltage: Equation (74)
     - Compute $\mathbf{G}^{\mathrm{ME}}$: Equation (63)
   - e) Evaluate residual: Equation (70)

6. Update time step and return to 1.
   $n \leftarrow n + 1$

where the vectors $\mathbf{g}_a$ and $\mathbf{g}_b$ are defined in Equations (64).

Finally, the new system obtained is simply given by:

$$\mathbf{M}\ddot{\mathbf{q}}_{n+1}^{\mathrm{M}} + \mathbf{F}^{\mathrm{M}}(\mathbf{q}_{n+1}^{\mathrm{M}}) + c_v \mathbf{F}_c^{\mathrm{M}}(\mathbf{q}_{n+1}^{\mathrm{M}}) + \mathbf{F}_{\mathrm{S}}^{\mathrm{ME}}(\mathbf{q}_{n+1}^{\mathrm{M}}) = \mathbf{G}_{n+1}^{\mathrm{M}} + \mathbf{G}_{n+1}^{\mathrm{ME}} + \mathbf{G}_{n+1}^{\mathrm{V}}. \tag{68}$$

Note that the resolution of this problem does not require the use of electrical degrees-of-freedom since after their elimination, only $\mathbf{q}^{\mathrm{M}}$ is involved in the numerical simulation.

5.8. Algorithm

In order to solve the non-linear problem (68), a combined Newmark (average acceleration) / Newton–Raphson scheme is used. This predictor-corrector algorithm works like a classical scheme. The difference lies in the calculation of the terms arising from the viscoelastic core. The dissipative force is evaluated before the iteration loop, while the internal memory force vector is updated at each time step after the iteration loop (or after convergence).

For the sake of clarity, the algorithm is illustrated in Table 1. In the prediction step, displacement, velocity and acceleration vectors are expressed by:

$$\mathbf{q}_{n+1}^{p} = \mathbf{q}_n + \Delta t \dot{\mathbf{q}}_n + (0.5 - \beta)\Delta t^2 \ddot{\mathbf{q}}_n \tag{69a}$$

$$\dot{\mathbf{q}}_{n+1}^{p} = \dot{\mathbf{q}}_n + (1-\gamma)\Delta t\ddot{\mathbf{q}}_n \tag{69b}$$

$$\ddot{\mathbf{q}}_{n+1}^{p} = \mathbf{0}. \tag{69c}$$

We note that the acceleration is chosen to be zero in order to obtain a stable iterative procedure (Géradin and Rixen, 1997).

The dissipative load is then calculated using Equation (58) and the residual vector can be evaluated as:

$$\mathbf{R}_{n+1} = \mathbf{M}\ddot{\mathbf{q}}_{n+1} + \mathbf{F}^{*}(\mathbf{q}_{n+1}) - \mathbf{G}_{n+1}^{*} \tag{70}$$

where $\mathbf{F}^{*} = \mathbf{F}^{\mathrm{M}} + c_v\mathbf{F}_c^{\mathrm{M}} + \mathbf{F}_{\mathrm{S}}^{\mathrm{ME}}$ and $\mathbf{G}^{*} = \mathbf{G}^{\mathrm{M}} + \mathbf{G}^{\mathrm{ME}} + \mathbf{G}^{\mathrm{V}}$.

The succeeding step consists of evaluating the norm of the residual vector, which has to satisfy a convergence criterion. If this condition holds, the internal memory force vector is updated through Equation (59). Otherwise, the iterative procedure is applied. We start by calculating the iteration matrix $\mathbf{S}$ such that:

$$\mathbf{S} = \mathbf{K}_{\mathrm{T}} + \frac{1}{\beta\Delta t^2}\mathbf{M} \tag{71}$$

which is used to compute the correction of the solution by the following expression:

$$\mathbf{S}(\mathbf{q}_{n+1})\Delta\mathbf{q} = -\mathbf{R}_{n+1} \tag{72}$$

where the displacement increment $\Delta\mathbf{q}$ is used to correct the solution by:

$$\mathbf{q}_{n+1} = \mathbf{q}_{n+1}^{p} + \Delta\mathbf{q} \tag{73a}$$

$$\dot{\mathbf{q}}_{n+1} = \dot{\mathbf{q}}_{n+1}^{p} + \frac{\gamma}{\beta\Delta t}\Delta\mathbf{q} \tag{73b}$$

$$\ddot{\mathbf{q}}_{n+1} = \ddot{\mathbf{q}}_{n+1}^{p} + \frac{1}{\beta\Delta t^2}\Delta\mathbf{q}. \tag{73c}$$

After this, the electromechanical coupling is taken into account by means of a feedback derivative control law, which is applied to link the piezoelectric patches. This means that the voltage measured in the actuator is directly proportional to the time derivative of the voltage induced in the sensor:

$$V^{\mathrm{A}} = -K_d\dot{V}^{\mathrm{S}} \tag{74}$$

where K_d is the derivative control gain constant. Further, the time derivative of the sensor voltage is computed by the Euler-backward approximation:

$$\dot{V}_{n+1}^{\mathrm{S}} = \frac{V_{n+1}^{\mathrm{S}} - V_n^{\mathrm{S}}}{\Delta t}. \tag{75}$$

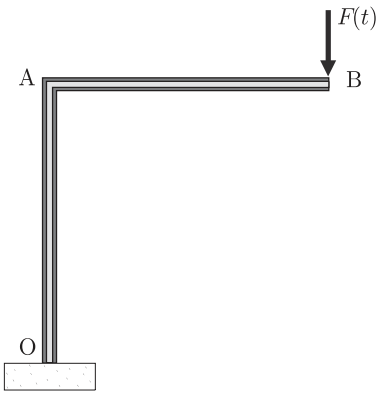

Figure 3. Sandwich frame (Deng and Vu-Quoc, 1998).

In this part of the algorithm, the piezoelectric internal force vector associated to a sensor configuration $\mathbf{F}_{\mathrm{S}}^{\mathrm{EM}}$ as well as the piezoelectric external force vector associated to an actuator configuration $\mathbf{G}^{\mathrm{ME}}$ have to be computed.

Finally, the equilibrium equation is evaluated to verify the convergence criterion.

6. RESULTS AND ANALYSIS

Two examples are presented in this section. The first one focuses on the validation of the sandwich beam formulation. It is an example extracted from Deng and Vu-Quoc (1998) where the authors propose an ideal sandwich frame formulation based on a Timoshenko beam theory. The second example deals with the attenuation of transient oscillations of a sandwich flexible robot arm by using hybrid active/passive damping treatment.

6.1. Sandwich Frame

Consider the sandwich frame shown in Figure 3. According to Deng and Vu-Quoc (1998), the three layers are supposed to be elastic and made with fictitious materials. Mechanical characteristics for the core (light gray layer) are given by $\rho_c = 1$, $c_{11}^c = 10^3$ and $c_{55}^c = 2 \times 10^3$ and for the faces (dark gray layer), $\rho_k = 20$ and $c_{11}^k = 4 \times 10^5$ (in a suitable unit system). Concerning geometrical data, length and width of the frame are OA = AB = 10 and $b = 1$, respectively. Moreover, the thickness of the core is $h_c = 1$ and a symmetrical configuration is assumed with $h_a = h_b = 0.05$.

The sandwich frame is discretized by a regular mesh of twenty finite elements: ten through OA and ten through AB. The calculations are performed using a time step equal to $\Delta t = 0.025$. The structure is clamped in O and submitted to an impact load at B. This force is described by a Heaviside function such as:

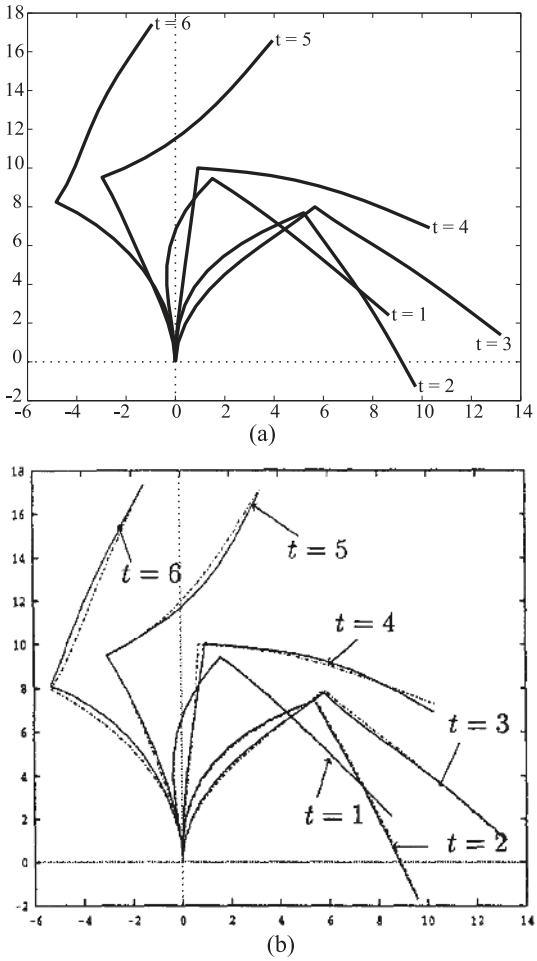

Figure 4. Sandwich-frame deformed shapes at different time steps: (a) present work and (b) Deng and Vu-Quoc (1998).

$$F(t) = \begin{cases} -1000 & \text{if} \quad 0 \leq t \leq 0.5 \\ \\ 0 & \text{if} \quad t > 0.5. \end{cases}$$

In Figure 4, the deformed shapes of the sandwich frame are presented for different instants (each 40 time steps) up to $T = 6$. It can be noted that the present results (Figure 4(a)) are very close to the reference solution developed by Deng and Vu-Quoc (1998) (Figure 4(b)).

Another set of results are depicted in Figure 5. They represent the time history of the axial and transverse displacements and rotations at point B. In the first row, axial (dashed line) and transverse displacements (solid line) obtained by using the present formulation Figure 5(a.1) are compared to the results obtained by Deng and Vu-Quoc (1998) Figure 5(a.2).

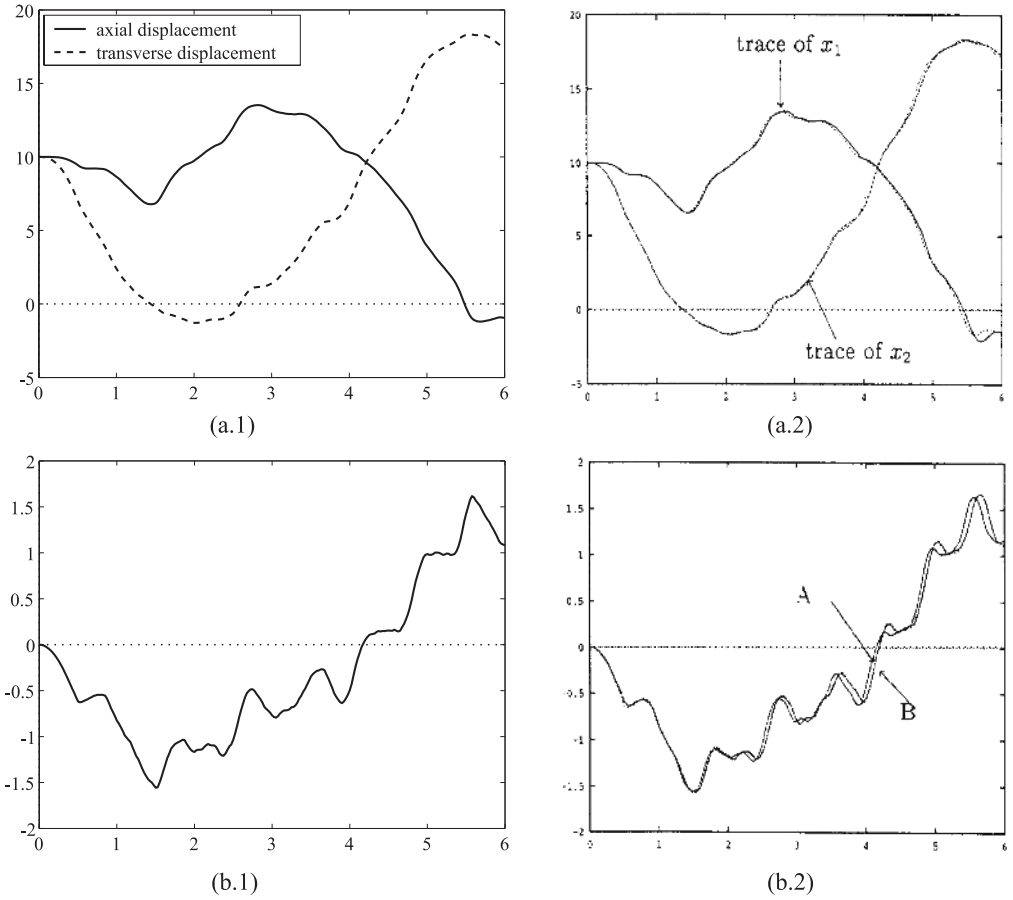

Figure 5. Time history of (a) axial and transverse tip displacements and (b) rotations at tip, where 1 stands for present work and 2 for Deng and Vu-Quoc (1998).

In the second row, the rotations are compared. In both cases, the present results are in very good agreement with those presented by Deng and Vu-Quoc (1998). Therefore, this example allows the validation of the (i) non-linear sandwich beam formulation without taking account of the viscoelastic/piezoelectric effects and (ii) the numerical predictor-corrector algorithm.

6.2. Sandwich Flexible Robot Arm

Consider a sandwich robot arm rotating in the plan $(x,\ z)$. A rotation is imposed on one of its ends, which is simply supported, the other end being free (see Figure 6). Mechanical characteristics of the materials used herein are shown in Table 2, noting that the four parameters of the viscoelastic model have been identified in Galucio et al. (2004).

The length of the arm is OA $=$ 250 mm and that one of the piezoelectric patches is 50 mm, with a common width of $b = 10$ mm. The position of the piezoelectric patch is such that its center is situated 75 mm to the right of point O. Twenty-five regular finite

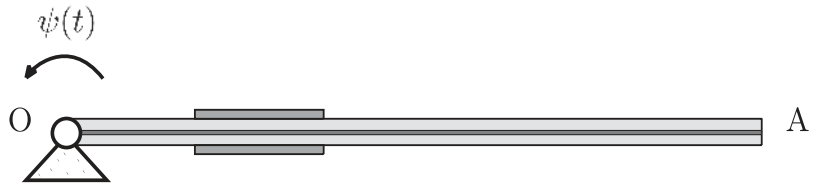

Figure 6. Sandwich flexible robot arm.

Table 2. Mechanical/electrical characteristics of different materials.

Aluminum	$\rho = 2690$ kg$/m^3$ $\quad \nu = 0.345 \quad E = 70.3$ GPa
PZT5H	$\rho = 7500$ kg/m^3 $\quad c_{11} = c_{33} = 126$ GPa $\quad c_{13} = 84.1$ GPa $e_{31} = -6.5$ C/m^2 $\quad e_{33} = 23.3$ C/m^2 $\quad d_{33} = 1,3 \times 10^{-8}$ F/m
ISD112 at 27°C	$\rho = 1600$ kg/m^3 $\quad \nu = 0.5 \quad E_o = 1.5$ MPa $\quad E_\infty = 69.95$ MPa $\alpha = 0.7915 \quad \tau = 1.4052 \times 10^{-2}$ ms

elements are used to discretize the beam: five between the point O and the left-end side of the piezoelectric patch, five along the patch and fifteen elsewhere. A feedback derivative control law is applied to the piezoelectric patches. Moreover, the structure is submitted to a prescribed rotation such that

$$\psi(t) = \begin{cases} \dfrac{\psi_o t}{t_1} & \text{if} \quad 0 \le t \le t_1 \\ \\ \psi_o & \text{if} \quad t_1 \le t \le T \end{cases}$$

where $t_1 = 20$ ms, $T = 200$ ms and $\psi_o = \pi/2$ rad. The time step used in the calculations is equal to $\Delta t = 0.02$ ms.

The geometry of the example is shown in Figure 6. The core is supposed to be viscoelastic (ISD112 at 27°C) constrained by elastic faces (aluminum) supplied with piezoelectric patches (PZT5H). The thickness distribution is 0.1, 1.5, and 0.5 (in mm) for the viscoelastic core, elastic faces and piezoelectric patches respectively.

Figure 7 presents the responses of the sandwich arm for a control gain $K_d = -10^{-3}$ ms. In the first row of the figure, the phase-space diagrams are depicted for axial (a) and transverse (b) tip displacements. The second row shows the corresponding displacement evolution in time. After 20 ms, i.e. the positioning time, the oscillations can be clearly observed in the space-phase diagrams to be successively attenuated. It should be emphasized that due to the large number of parameters involved in this non-linear problem, an experimental validation might be necessary in order to obtain the best values of geometry, integration parameters and so on. The present formulation allows one to treat non-linear dynamics with coupled systems without further numerical effort.

Finally, the number of iterations required to achieve convergence does not exceed four, which is a reasonable number. Obviously, this number depends on several parameters, espe-

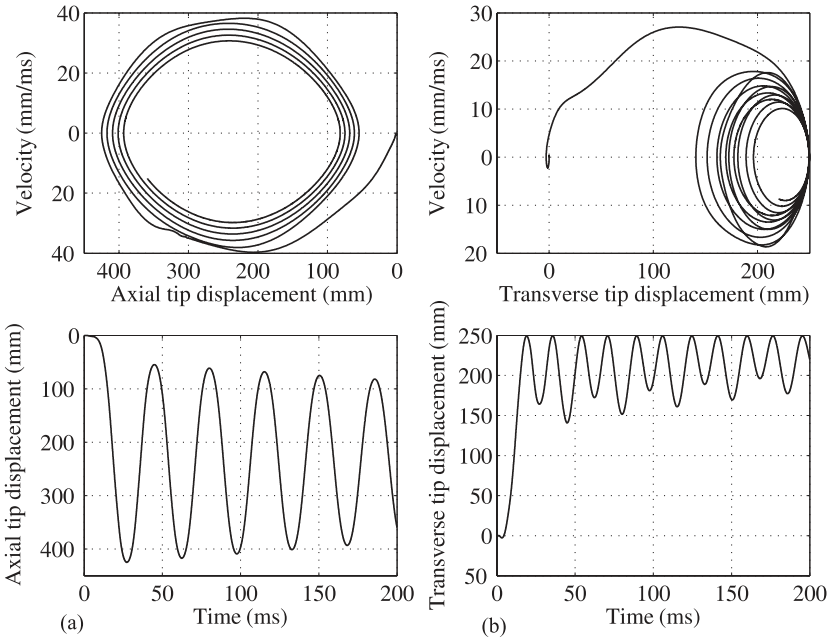

Figure 7. Axial (a) and transverse (b) space-phase diagrams and tip displacements of the sandwich arm.

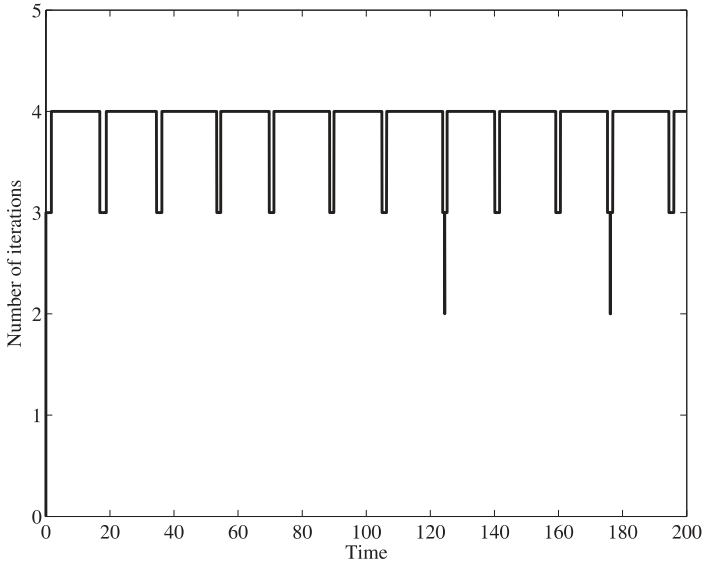

Figure 8. Number of iterations to achieve convergence.

cially on the time discretization. Therefore, a set of numerical tests should be performed in order to optimize the computational time for this kind of problem.

7. CONCLUSIONS

A co-rotational finite element formulation of an adaptive sandwich beam composed of a viscoelastic core constrained by laminated elastic/piezoelectric faces is proposed. The four-parameter fractional Zener model is used to take the linear viscoelastic behavior of the middle layer into account, while a three-dimensional classical piezoelectric constitutive law is used for modeling the piezoelectric material.

The finite element formulation allows large displacements and rotations with a local small strain measure. Local electrical degrees-of-freedom are used in order to reproduce sensor configurations. A static condensation is performed at elementary level in order to eliminate electrical degrees-of-freedom to solve a mechanic system. Concerning the viscoelastic damping, fractional derivative operators are approximated by the Grünwald–Letnikov scheme, where the history of the internal memory force is used to take account of the damping effect.

The classical Newmark/Newton–Raphson predictor-corrector algorithm is slightly modified to solve the non-linear dynamic problem. The internal memory force vector is updated at each time step after convergence of the solution. A feedback derivative control law is used to take the piezoelectric effect into account.

An example validation is performed showing very good agreement between the present method and the reference solution. Finally, the transient responses of a sandwich flexible robot arm are attenuated through passive and active/passive damping treatments.

A. TRANSFORMATION MATRIX

As previously mentioned, the relation between the virtual local and global displacement vectors is such that $\delta\mathbf{q}\cdot = \mathbf{T}\delta\mathbf{q}$, where $\mathbf{T}$ is the transformation matrix defined as:

$$\mathbf{T} = [\ \mathbf{T}_1 \quad \mathbf{T}_2 \quad \mathbf{T}_3 \quad \mathbf{T}_4 \quad \mathbf{T}_5 \quad \mathbf{T}_6 \quad \mathbf{T}_7 \quad \mathbf{T}_8\ ]^{\mathrm{T}} \tag{76}$$

with its row-matrices given by:

$$\mathbf{T}_1 = \frac{h_1}{\ell}\mathbf{z}^{\mathrm{T}} + [\ 0 \quad 0 \quad -h_1 \quad 0 \quad 0 \quad 0 \quad 0 \quad 0 \quad 0 \quad 0\ ] \tag{77a}$$

$$\mathbf{T}_2 = -\frac{1}{\ell}\mathbf{z}^{\mathrm{T}} + [\ 0 \quad 0 \quad 1 \quad 0 \quad 0 \quad 0 \quad 0 \quad 0 \quad 0 \quad 0\ ] \tag{77b}$$

$$\mathbf{T}_3 = \frac{h_2}{\ell}\mathbf{z}^{\mathrm{T}} + [\ 0 \quad 0 \quad 0 \quad 1 \quad 0 \quad 0 \quad 0 \quad 0 \quad 0 \quad 0\ ] \tag{77c}$$

$$\mathbf{T}_4 = \mathbf{r}^{\mathrm{T}} + \frac{h_1}{\ell}\mathbf{z}^{\mathrm{T}} + [\ 0 \quad 0 \quad 0 \quad 0 \quad 0 \quad 0 \quad -h_1 \quad 0 \quad 0 \quad 0\ ] \tag{77d}$$

$$\mathbf{T}_5 = -\frac{1}{\ell}\mathbf{z}^{\mathrm{T}} + [\ 0 \quad 0 \quad 0 \quad 0 \quad 0 \quad 0 \quad 1 \quad 0 \quad 0 \quad 0\ ] \tag{77e}$$

$$\mathbf{T}_6 = \frac{h_2}{\ell}\mathbf{z}^{\mathrm{T}} + [\ 0\ \ 0\ \ 0\ \ 0\ \ 0\ \ 0\ \ 0\ \ 1\ \ 0\ \ 0\ ] \tag{77f}$$

$$\mathbf{T}_7 = [\ 0\ \ 0\ \ 0\ \ 0\ \ 0\ \ 0\ \ 0\ \ 0\ \ 1\ \ 0\ ] \tag{77g}$$

$$\mathbf{T}_8 = [\ 0\ \ 0\ \ 0\ \ 0\ \ 0\ \ 0\ \ 0\ \ 0\ \ 0\ \ 1\ ] \tag{77h}$$

where the vectors $\mathbf{r}$ and $\mathbf{z}$ are respectively defined in Equations (29) and (33).

B. LOCAL INTERNAL FORCE VECTOR

Let us recall the definition of the internal force vector written in local coordinate system:

$$\delta U = \delta\hat{\mathbf{q}}^{\mathrm{T}}\hat{\mathbf{F}}$$

where viscoelastic and piezoelectric contributions are taken into account through $\hat{\mathbf{F}}$, in accordance with Equation (43). Hence, each contribution of $\hat{\mathbf{F}}$ is given below.

B1. Components of $\hat{\mathbf{F}}$

B.1.1. Mechanical internal force vectors

The mechanical contribution of the internal force vector is derived from the discretization of Equations (15a) and (16) such that:

$$\hat{\mathbf{F}}^{\mathrm{M}} = \hat{\mathbf{F}}^{\mathrm{M}}_a + \hat{\mathbf{F}}^{\mathrm{M}}_b + (1 + c_v)\hat{\mathbf{F}}^{\mathrm{M}}_c. \tag{78}$$

Note that the mechanical contribution associated with the core arises solely from the discretization of the first term of the right-hand side of Equation (16). The other term, which depends on the history of the internal memory force vector, is treated as an external loading following Section 5.7.

After discretizing Equation (15a), the mechanical contribution of the internal force vector for the laminated faces becomes:

$$\hat{\mathbf{F}}^{\mathrm{M}}_a = \frac{\bar{c}^a_{11}A_a}{\ell_o}\begin{bmatrix} -\hat{\bar{u}}_{21} - \hat{\tilde{u}}_{21}/2 \\ 0 \\ -\hat{\bar{u}}_{21}/2 - \hat{\tilde{u}}_{21}/4 \\ \hat{\bar{u}}_{21} + \hat{\tilde{u}}_{21}/2 \\ 0 \\ \hat{\bar{u}}_{21}/2 + \hat{\tilde{u}}_{21}/4 \\ 0 \\ 0 \end{bmatrix} + \frac{\bar{c}^a_{11}I_a}{\ell_o}\begin{bmatrix} 0 \\ 4\hat{w}'_1 + 2\hat{w}'_2 \\ 0 \\ 0 \\ 2\hat{w}'_1 + 4\hat{w}'_2 \\ 0 \\ 0 \\ 0 \end{bmatrix} \tag{79a}$$

$$\hat{\mathbf{F}}_b^{\mathrm{M}} = \frac{\bar{c}_{11}^b A_b}{\ell_o} \begin{bmatrix} -\hat{\tilde{u}}_{21} + \hat{\tilde{u}}_{21}/2 \\ 0 \\ \hat{\tilde{u}}_{21}/2 - \hat{\tilde{u}}_{21}/4 \\ \hat{\tilde{u}}_{21} - \hat{\tilde{u}}_{21}/2 \\ 0 \\ -\hat{\tilde{u}}_{21}/2 + \hat{\tilde{u}}_{21}/4 \\ 0 \\ 0 \end{bmatrix} + \frac{\bar{c}_{11}^b I_b}{\ell_o} \begin{bmatrix} 0 \\ 4\hat{w}_1' + 2\hat{w}_2' \\ 0 \\ 0 \\ 2\hat{w}_1' + 4\hat{w}_2' \\ 0 \\ 0 \\ 0 \end{bmatrix}. \tag{79b}$$

For the middle layer, the partial discretization of Equation (16) allows one to write the mechanical internal force vector associated with the core as:

$$\hat{\mathbf{F}}_c^{\mathrm{M}} = \hat{\mathbf{F}}_{mc}^{\mathrm{M}} + \hat{\mathbf{F}}_{bc}^{\mathrm{M}} + \hat{\mathbf{F}}_{sc}^{\mathrm{M}} \tag{80}$$

where its membrane, bending and shear components are given by:

$$\hat{\mathbf{F}}_{mc}^{\mathrm{M}} = \frac{\bar{c}_{11}^c A_c h_1}{\ell_o} \begin{bmatrix} -\hat{\tilde{u}}_{21}/h_1 - \hat{w}_{21}' \\ -\hat{\tilde{u}}_{21} + 2h_1\left(2\hat{w}_1' + \hat{w}_2'\right) \\ 0 \\ \hat{\tilde{u}}_{21}/h_1 + \hat{w}_{21}' \\ \hat{\tilde{u}}_{21} + 2h_1\left(\hat{w}_1' + 2\hat{w}_2'\right) \\ 0 \\ 0 \\ 0 \end{bmatrix} \tag{81a}$$

$$\hat{\mathbf{F}}_{bc}^{\mathrm{M}} = \frac{\bar{c}_{11}^c I_c}{\ell_o} \frac{h_2 - h_c}{h_c^2} \begin{bmatrix} 0 \\ 2(h_2 - h_c)(2\hat{w}_1' + \hat{w}_2') - \hat{\tilde{u}}_{21} \\ -\hat{w}_{21}' - \hat{\tilde{u}}_{21}/(h_2 - h_c) \\ 0 \\ 2(h_2 - h_c)(\hat{w}_1' + 2\hat{w}_2') + \hat{\tilde{u}}_{21} \\ \hat{w}_{21}' + \hat{\tilde{u}}_{21}/(h_2 - h_c) \\ 0 \\ 0 \end{bmatrix} \tag{81b}$$

$$\hat{\mathbf{F}}^{\mathrm{M}}_{sc} = \frac{\bar{c}^{c}_{55} k_c A_c \ell_o h_2}{12 h_c^2} \begin{bmatrix} 0 \\ 2h_2(4\hat{w}'_1 - \hat{w}'_2)/5 - \hat{\tilde{u}}_{21} \\ -\hat{w}'_{21} + 2(2\hat{\tilde{u}}_1 + \hat{\tilde{u}}_2)/h_2 \\ 0 \\ -2h_2(\hat{w}'_1 - 4\hat{w}'_2)/5 + \hat{\tilde{u}}_{21} \\ \hat{w}'_{21} + 2(\hat{\tilde{u}}_1 + 2\hat{\tilde{u}}_2)/h_2 \\ 0 \\ 0 \end{bmatrix}. \tag{81c}$$

B.1.2. Piezoelectric internal force vectors

The electromechanical internal force vector arising from the discretization of Equation (15b) depends simply on the voltage applied (or induced) at each piezoelectric layer:

$$\hat{\mathbf{F}}^{\mathrm{ME}}_{a} = \frac{\bar{e}^{a}_{31} A_a}{h_a} \begin{bmatrix} -\hat{V}_a & 0 & -\hat{V}_a/2 & \hat{V}_a & 0 & \hat{V}_a/2 & 0 & 0 \end{bmatrix}^{\mathrm{T}} \tag{82a}$$

$$\hat{\mathbf{F}}^{\mathrm{ME}}_{b} = \frac{\bar{e}^{b}_{31} A_b}{h_b} \begin{bmatrix} -\hat{V}_b & 0 & \hat{V}_b/2 & \hat{V}_b & 0 & -\hat{V}_b/2 & 0 & 0 \end{bmatrix}^{\mathrm{T}} \tag{82b}$$

whereas the one computed using Equation (15c) depends on the mechanical axial displacements:

$$\hat{\mathbf{F}}^{\mathrm{EM}}_{a} = \frac{\bar{e}^{a}_{31} A_a}{h_a} \begin{bmatrix} 0 & 0 & 0 & 0 & 0 & 0 & \hat{\tilde{u}}_{21} + \hat{\tilde{u}}_{21}/2 & 0 \end{bmatrix}^{\mathrm{T}} \tag{83a}$$

$$\hat{\mathbf{F}}^{\mathrm{EM}}_{b} = \frac{\bar{e}^{b}_{31} A_b}{h_b} \begin{bmatrix} 0 & 0 & 0 & 0 & 0 & 0 & 0 & \hat{\tilde{u}}_{21} - \hat{\tilde{u}}_{21}/2 \end{bmatrix}^{\mathrm{T}}. \tag{83b}$$

B.1.3. Dielectric internal force vectors

The dielectric contribution of the internal force vector is obtained from the discretized form of Equation (15d). This results in the following expressions:

$$\hat{\mathbf{F}}^{\mathrm{E}}_{a} = \frac{\bar{d}^{a}_{33} A_a \ell_o}{h_a^2} \begin{bmatrix} 0 & 0 & 0 & 0 & 0 & 0 & -\hat{V}_a & 0 \end{bmatrix}^{\mathrm{T}} \tag{84a}$$

$$\hat{\mathbf{F}}^{\mathrm{E}}_{b} = \frac{\bar{d}^{b}_{33} A_b \ell_o}{h_b^2} \begin{bmatrix} 0 & 0 & 0 & 0 & 0 & 0 & 0 & -\hat{V}_b \end{bmatrix}^{\mathrm{T}}. \tag{84b}$$

C. MATERIAL STIFFNESS MATRIX

C1. Components of $\hat{\mathbf{K}}$

Recall that the material stiffness matrix, which was previously defined by Equation (50), depends on the matrix transformation given in Appendix A and on the following (8×8)-matrix:

$$\hat{\mathbf{K}} = \begin{bmatrix} \hat{K}_{11} & \hat{K}_{12} & \hat{K}_{13} & -\hat{K}_{11} & -\hat{K}_{12} & -\hat{K}_{13} & \hat{K}_{17} & \hat{K}_{18} \\ & \hat{K}_{22} & \hat{K}_{23} & -\hat{K}_{12} & \hat{K}_{25} & -\hat{K}_{23} & 0 & 0 \\ & & \hat{K}_{33} & -\hat{K}_{13} & -\hat{K}_{23} & \hat{K}_{36} & \hat{K}_{37} & \hat{K}_{38} \\ & & & \hat{K}_{11} & \hat{K}_{12} & \hat{K}_{13} & -\hat{K}_{17} & -\hat{K}_{18} \\ & \text{symm} & & & \hat{K}_{22} & \hat{K}_{23} & 0 & 0 \\ & & & & & \hat{K}_{33} & -\hat{K}_{37} & -\hat{K}_{38} \\ & & & & & & \hat{K}_{77} & 0 \\ & & & & & & & \hat{K}_{88} \end{bmatrix} \tag{85}$$

where its fourteen independent components, written in terms of geometric and material properties, are defined by:

$$\hat{K}_{11} = \frac{1}{\ell_o}\left[\bar{c}^a_{11}A_a + \bar{c}^b_{11}A_b + (1+c_v)\bar{c}^c_{11}A_c\right] \tag{86a}$$

$$\hat{K}_{12} = (1+c_v)\frac{\bar{c}^c_{11}A_c h_1}{\ell_o} \tag{86b}$$

$$\hat{K}_{13} = \frac{1}{2\ell_o}(\bar{c}^a_{11}A_a - \bar{c}^b_{11}A_b) \tag{86c}$$

$$\hat{K}_{17} = -\frac{\bar{e}^a_{31}A_a}{h_a} \tag{86d}$$

$$\hat{K}_{18} = -\frac{\bar{e}^b_{31}A_b}{h_b} \tag{86e}$$

$$\begin{aligned} \hat{K}_{22} &= \frac{4}{\ell_o}\left(\bar{c}^a_{11}I_a + \bar{c}^b_{11}I_b\right) \\ &+ (1+c_v)\left\{\frac{4\bar{c}^c_{11}}{\ell_o}\left[I_c\left(\frac{h_2}{h_c}-1\right)^2 + A_c h_1^2\right] + \frac{2\bar{c}^c_{55}A_c h_2^2 \ell_o}{15h_c^2}\right\} \end{aligned} \tag{86f}$$

$$\hat{K}_{23} = (1+c_v)\left[\frac{\bar{c}^c_{11}I_c}{h_c\ell_o}\left(\frac{h_2}{h_c}-1\right) + \frac{\bar{c}^c_{55}A_c h_2 \ell_o}{12h_c^2}\right] \tag{86g}$$

$$\hat{K}_{25} = \frac{2}{\ell_o}(\bar{c}^a_{11} I_a + \bar{c}^b_{11} I_b)$$
$$+ (1+c_v)\left\{\frac{2\bar{c}^c_{11}}{\ell_o}\left[I_c\left(\frac{h_2}{h_c}-1\right)^2 + A_c h_1^2\right] - \frac{\bar{c}^c_{55} A_c h_2^2 \ell_o}{30 h_c^2}\right\} \quad (86h)$$

$$\hat{K}_{33} = \frac{1}{4\ell_o}(\bar{c}^a_{11} A_a + \bar{c}^b_{11} A_b) + (1+c_v)\left(\frac{\bar{c}^c_{11} I_c}{h_c^2 \ell_o} + \frac{\bar{c}^c_{55} A_c \ell_o}{3h_c^2}\right) \quad (86i)$$

$$\hat{K}_{36} = -\frac{1}{4\ell_o}(\bar{c}^a_{11} A_a + \bar{c}^b_{11} A_b) - (1+c_v)\left(\frac{\bar{c}^c_{11} I_c}{h_c^2 \ell_o} - \frac{\bar{c}^c_{55} A_c \ell_o}{6h_c^2}\right) \quad (86j)$$

$$\hat{K}_{37} = -\frac{\bar{e}^a_{31} A_a}{2h_a} \quad (86k)$$

$$\hat{K}_{38} = \frac{\bar{e}^b_{31} A_b}{2h_b} \quad (86l)$$

$$\hat{K}_{77} = -\frac{\bar{d}^a_{33} A_a \ell_o}{h_a} \quad (86m)$$

$$\hat{K}_{88} = -\frac{\bar{d}^b_{33} A_b \ell_o}{h_b}. \quad (86n)$$

Acknowledgments. This research is partially carried out within the 6th Framework Programme of the European Commission (InMAR project) under Grant No. NMP2-CT-2003-501084.

REFERENCES

Adolfsson, K., Enelund, M., and Larsson, S., 2004, "Adaptive discretization of fractional order viscoelasticity using sparse time history," *Computer Methods in Applied Mechanics and Engineering* **193**, 4567–4590.

Bagley, R.L. and Torvik, P.J., 1983, "Fractional calculus – a different approach to the analysis of viscoelastically damped structures," *AIAA Journal* **21**, 741–748.

Baz, A., 1996, "Active constrained layer damping," US Patent 5,485,053.

Baz, A. and Ro, J., 1996, "Vibration control of plates with active constrained layer damping," *Journal of Smart Materials and Structures* **5**, 272–280.

Baz, A. and Ro, J., 2001, "Vibration control of rotating beams with active constrained layer damping," *Journal of Smart Materials and Structures* **10**, 112–120.

Belytschko, T. and Hsieh, B.J., 1973, "Non-linear transient finite element analysis with convected co-ordinates," *International Journal for Numerical Methods in Engineering* **7**, 255–271.

Chen, J.-S. and Huang, C.-L., 2001, "Dynamic analysis of flexible slider-crank mechanisms with non-linear finite element method," *Journal of Sound and Vibration* **246**(3), 389–402.

Deng, H. and Vu-Quoc, L., 1998, "Dynamics of geometrically exact sandwich structures," *International Journal of Mechanical Sciences* **40**, 421–441.

Diethelm, K., Ford, N.J., and Freed, A.D., 2004, "Detailed error analysis for a fractional Adams method," *Numerical Algorithms* **36**, 31–52.

Felippa, C.A. and Haugen, B., 2005, "A unified formulation of small-strain corotational finite elements: I. Theory," *Computer Methods in Applied Mechanics and Engineering* **194**, 2285–2335.

Fung, E.H.K. and Yau, D.T.W., 2004, "Vibration characteristics of a rotating flexible arm with ACLD treatment," *Journal of Sound and Vibration* **269**, 165–182.

Galucio, A.C., Deü, J.-F., and Ohayon, R., 2004, "Finite element formulation of viscoelastic sandwich beams using fractional derivative operators," *Computational Mechanics* **33**, 282–291.

Galucio, A.C., Deü, J.-F., Mengué, S., and Dubois, F., 2006, "An adaptation of the Gear scheme for fractional derivatives," *Computer Methods in Applied Mechanics and Engineering* **195**, 6073–6085.

Géradin, M. and Rixen, D., 1997, *Mechanical Vibrations*. John Wiley and Sons.

Hsiao, K.-M. and Jang, J.-Y., 1991, "Dynamic analysis of planar flexible mechanisms by co-rotational formulation," *Computer Methods in Applied Mechanics and Engineering* **87**, 1–14.

Iura, M. and Atluri, S.N., 1995, "Dynamic analysis of planar flexible beams with finite rotations by using inertial and rotating frames," *Computers and Structures* **55**(3), 453–462.

Jonker, B., 1989, "A finite element dynamic analysis of spatial mechanisms with flexible links," *Computer Methods in Applied Mechanics and Engineering* **76**, 17–40.

Lin, C.-Y. and Chen, L.-W., 2003 "Dynamic stability of a rotating beam with a constrained damping layer," *Journal of Sound and Vibration* **267**, 209–225.

Meek, J.L. and Liu, H., 1995, "Nonlinear dynamics analysis of flexible beams under large overall motions and the flexible manipulator simulation," *Computers and Structures* **56**(1), 1–14.

Preiswerk, M. and Venkatesh, A., 1994, "An analysis of vibration control using piezoceramics in planar flexible-linkage mechanisms," *Journal of Smart Materials and Structures* **3**, 190–200.

Shi, G. and Atluri, S.N., 1990, "Active control of nonlinear dynamic response of space-frames using piezo-electric actuators," *Computers and Structures* **34**(4), 549–564.

Simo, J.C. and Vu-Quoc, L., 1986, "On the dynamics of flexible beams under large overall motions – the plane case: Part I and Part II," *Journal of Applied Mechanics* **53**, 849–863.

Simo, J.C. and Vu-Quoc, L., 1988, "On the dynamics in space of rods undergoing large motions – a geometrically exact approach," *Computer Methods in Applied Mechanics and Engineering* **66**, 125–161.

Sun, D. and Tong, L., 2004, "A compressional-shear model for vibration control of beams with active constrained layer damping," *International Journal of Mechanical Sciences* **46**, 1307–1325.

Tan, X.G. and Vu-Quoc, L., 2005, "Optimal solid shell element for large deformable composite structures with piezoelectric layers and active vibration control," *International Journal for Numerical Methods in Engineering* **64**, 1981–2013.

Zhang, X. and Erdman, A.G., 2001, "Dynamic responses of flexible linkage mechanisms with viscoelastic constrained layer damping treatment," *Computers and Structures* **79**, 1265–1274.